

4th order tensors for multi-fiber resolution and segmentation in white matter

Temesgen Bihonegn, Avinash Bansal, Sumit Kaushik, Jan Slovák
Departement of Mathematics and Statistics
Masaryk University, Brno, Czech Republic

Abstract—Since its inception, DTI modality has become an essential tool in the clinical scenario. In principle, it is rooted in the emergence of symmetric positive definite (SPD) second-order tensors modelling the diffusion. The inability of DTI to model regions of white matter with fibers crossing/merging leads to the emergence of higher order tensors. In this work, we compare various approaches how to use 4th order tensors to model such regions. There are three different projections of these 3D 4th order tensors to the 2nd order tensors of dimensions either three or six. Two of these projections are consistent in terms of preserving mean diffusivity and isometry. The images of all three projections are SPD, so they belong to a Riemannian symmetric space. Following previous work of the authors, we use the standard k-means segmentation method after dimension reduction with affinity matrix based on reasonable similarity measures, with the goal to compare the various projections to 2nd order tensors. We are using the natural affine and log-Euclidean (LogE) metrics. The segmentation of curved structures and fiber crossing regions is performed under the presence of several levels of Rician noise. The experiments provide evidence that 3D 2nd order reduction works much better than the 6D one, while diagonal components (DC) projections are able to reveal the maximum diffusion direction.

I. INTRODUCTION

Based upon NMR principles Lauterbur, [1], developed MRI technique to render 3D images. Diffusion-weighted images have come a long way since then. Diffusion Tensor Imaging (DTI) was introduced to model diffusion in biological tissues in [2] and [3]. It proved phenomenal in clinical studies to probe into cerebral white matter structures. It enabled us to infer the microstructures of tissues in vivo and noninvasively. The introduction of more diffusion gradient directions revealed more detailed structures (in DTI the number of independent parameters for each voxel is six). This acquisition protocol is known as high angular diffusion imaging (HARDI). Since then various modalities based upon HARDI have been proposed [4][5]. The monoexponential Stejskal-Tanner equation is assumed to model the D-MRI (Diffusion-Magnetic Resonance Imaging) principle. The DTI model is restricted to produce second-order tensors. These tensors are effective in modeling the regions where fibers are not crossing, merging or touching. These SPD tensors are known to live the Riemannian symmetric space of the positive definite quadrics. Various works have utilized this space for processing these tensors [6][7][8][9][10][11]. Another common approach is to use q-space like DSI and Q-Ball. Diffusion is a physical process, methods in [12][13] ensure the full symmetry and positive

definiteness of higher order tensors. Every symmetric tensor can be represented as a homogeneous polynomial [13]. This helps in finding the maxima of the Apparant Diffusion Coefficient (ADC) profiles. One reason to use higher order tensors is that they encode diffusion geometry without the need of evaluating spherical harmonics from the diffusion profiles. Another advantage comes from the observation that the computation of coefficients of lower-order tensors can be obtained from coefficients of higher-order tensor using linear relations [14][15] without refitting of DMR signal. The works in [16][17] suggest that in intersection regions these tensors fail to orient properly with the underlying direction of actual fibers. The issue of reorientation is resolved in work [17] and the approach is referred to as Cartesian Tensor-fiber orientation distribution (CT-FOD).

In [18][19], the authors approached the segmentation problem by considering the individual fiber bundles to lie in 1D/2D/3D subspaces, depending upon the numbers of the intersecting fibers. In [20], 5D non-linear geometry is employed to segregate fiber tracts. This approach proved advantageous over the 3D Euclidean space assumption. The surface evolution [21] in Riemannian space can segment such curved structures. Works [22][11] used the Hilbert sphere in infinite dimension and mapped the data to lower dimension for segmentation.

In this work, we discuss the order reduction of the 3D 4th order tensors. This reduction yields 2nd order tensors in 3D and 6D. Further, these reductions are SPDs and therefore lie in Riemannian symmetric space. These SPD data belong to a log-normal distribution. We computed the variance of the data using this property. Subsequently, a non-linear dimensionality reduction method known as Laplacian-Eigenmap clustering is utilized for the extraction of anisotropic regions in both synthetic and real images. The results infer that systematic order reduction of tensors is useful and it is robust under noise. We segmented with single and two crossing fibers with various complex configurations. Another observation is that the diagonal component projection obtained from flattened 3D 4th order tensor can reveal the direction of maximum diffusion. Our experiments are discussed in detail in section V.

II. BACKGROUND

A. Diffusion Modelling

The Stejskal-Tanner equation represents a mono-exponential model of water molecules diffusing in tissues

given by:

$$S(b, v) = S_0 \exp(-bD(v)),$$

$$D(v) = \sum_{j_1=1}^3 \sum_{j_2=1}^3 \sum_{j_3=1}^3 \dots \sum_{j_n=1}^3 D_{j_1 j_2 j_3 \dots j_n} v^{j_1} v^{j_2} v^{j_3} \dots v^{j_n}, \quad (1)$$

where v_ℓ is ℓ th magnetic gradient component and $\|v\| = 1$. $S(v)$ is the attenuated signal when gradient pulse is applied and b is diffusion weighting coefficient. Due to antipodal symmetry and physicality of diffusion process, the higher order tensors from the above equation are positive definite and of even order. For the same reasons, these tensors are fully symmetric. Due to the full symmetry, the number of independent coefficients for k th order tensor is reduced from 3^k to $\frac{1}{2}(k+1)(k+2)$. The seminal work of Tuch et. al. [23] is based upon the conjuncture that increasing number of gradient directions should be able to reveal geometry of the biological tissues. For 4th order tensors, 81 coefficients reduce to 15.

B. Linear Algebra

Let V be n -dimensional vector space defined over real numbers \mathbb{R} . 4th order tensors form a vector space of dimension n^4 , where $n = 3$ in our case. We are interested in the so called Cartesian tensors, i.e., the coordinate description of the tensor in a fixed orthonormal basis of the vector space V . Thus, a second order tensor can be viewed as 2-dimensional array of scalars. Under orthogonal basis, tensors can be also represented as k -linear forms

$$T(X_1, \dots, X_k) = \sum_{j=1}^n T_{j_1 \dots j_k} x_1^{j_1} \dots x_k^{j_k} \quad (2)$$

where the tensor T is evaluated at vectors X_i . Using an orthonormal basis e^i , $i = 1, 2, \dots, n$, a 4th order tensor T is written as

$$T^{(4)} = \sum_{1 \leq i, j, k, l} T_{ijkl}^{(4)} e_i \otimes e_j \otimes e_k \otimes e_l, \quad (3)$$

where the individual terms $e_i \otimes e_j \otimes e_k \otimes e_l$ form the induced orthonormal basis of the space of fourth order tensors. Thus, there is the induced scalar product of two tensor $S = S_{i_1 \dots i_k}$, $R = R_{i_1 \dots i_k}$, cf. [24], the so called dot product

$$S \bullet R = \sum_{i_1, \dots, i_k} S_{i_1 \dots i_k} R^{i_1 \dots i_k}. \quad (4)$$

For $k = 2$, the scalar product of two tensors becomes

$$S \bullet R = \sum_{i, j=1}^n S_j^i R_i^j = \text{trace}(R^T S). \quad (5)$$

The corresponding Euclidean distance measure on the space of tensors becomes

$$d_E(S, R) = \|S - R\|. \quad (6)$$

Exploiting the inner product, the 4th order tensors can be identified as mappings between second order tensors.

This means, we can represent $T^{(4)}$ using 2nd order tensor components. For $1 \leq i, j, k, l \leq n$ we arrive at

$$T^{(4)} = \sum_{ijkl} T_{ijkl}^{(4)} e_i \otimes e_j \otimes e_k \otimes e_l = \sum_{IJ} T_{IJ}^{(2)} e_I \otimes e_J \quad (7)$$

where $e_{I(i,j)} = e_i \otimes e_j$, $e_{J(k,l)} = e_k \otimes e_l$. In view of this identification, they exhibit three types of symmetries:

- 1) Major Symmetry: $T_{ijkl} = T_{klij}$, $1 \leq i, j, k, l \leq n$, which corresponds to symmetric mappings between the second order tensors.
- 2) Minor Symmetry: $T_{ijkl} = T_{jikl} = T_{ijlk}$, which corresponds to the restriction to symmetric second order tensors, with symmetric values.
- 3) Total Symmetry: $T_{ijkl} = T_{\sigma(i)\sigma(j)\sigma(k)\sigma(l)}$, for every permutation σ , which means both of the previous symmetries together.

In diffusion process, the even order tensors obey total symmetry. These 3D 4th order tensors can be represented as homogeneous polynomials (say in coordinates x, y, z) of degree 4, built of monomials $p_{ijk} x^i y^j z^k$ with $i + j + k = 4$. The relation between the coefficient of the polynomial and that of tensor is represented by the equation: $\frac{i!j!k!}{4!} p_{ijk} = D_{j_1 j_2 j_3 j_4}$, where j_ℓ are one of the terms x, y, z . Vector representations of 4th order and 2nd order tensors are unable to reveal their geometric properties, like the distribution of eigenvalues and eigenvectors of the tensorial form [25]. By losing the tensorial form, it is not possible to see the effect of rotation of the coordinate system on the distribution of tensor [26], etc. For these reasons, we are interested in the reductions which are obtained systematically while preserving important information.

III. MAPPINGS

A. 6D 2nd order representation

The appearance of 4th order tensor is known in various fields [27][28]. In material science, they are known to classify materials based upon their elasticity [29][30][31]. They model the material symmetries, which is reflected in the invariance of components of the tensor with permutation of indices. A 3D 4th order tensor with minor symmetry can be written as Voigt contracted notation:

$$D = \begin{pmatrix} D_{xxxx} & D_{xxyy} & D_{xxzz} & \sqrt{2}D_{xxyz} & \sqrt{2}D_{xxzx} & \sqrt{2}D_{xxxy} \\ D_{yyxx} & D_{yyyy} & D_{yyzz} & \sqrt{2}D_{yyyz} & \sqrt{2}D_{yyzx} & \sqrt{2}D_{yyxy} \\ D_{zzxx} & D_{zzyy} & D_{zzzz} & \sqrt{2}D_{zzyz} & \sqrt{2}D_{zzzx} & \sqrt{2}D_{zzxy} \\ \sqrt{2}D_{yxxx} & \sqrt{2}D_{yzyy} & \sqrt{2}D_{yzzz} & D_{yzyz} & D_{yzzx} & D_{yzxy} \\ \sqrt{2}D_{zxxx} & \sqrt{2}D_{zzyy} & \sqrt{2}D_{zzzz} & D_{zxzy} & D_{zxzx} & D_{zxxy} \\ \sqrt{2}D_{xyxx} & \sqrt{2}D_{xyyy} & \sqrt{2}D_{xyzz} & D_{xyyz} & D_{xyzx} & D_{xyxy} \end{pmatrix}_{(8)}$$

With the following extra equalities the tensor exhibits the total symmetry.

$$\begin{aligned} D_{xxyy} &= D_{xyxy}, D_{xxzz} = D_{zxzx}, D_{yyzz} = D_{zyzy} \\ D_{xxyz} &= D_{xyxz}, D_{yyxz} = D_{xyyz}, D_{zzxy} = D_{xzyz} \end{aligned}$$

In this isometric notation, it is a 6D second order tensor. This tensor is an SPD and so, lies in Riemannian symmetric space. Their positive definiteness is a favourable property to justify diffusion as a physical phenomenon. The conversion between 3D 4th order tensor coefficient and 6D 2nd order is obtained through equation (8). The factor 2 and $\sqrt{2}$ ensures isomorphism between the two spaces [32][33].

B. 3D 2nd order reduction

There are many ways to represent the 4th order tensor. An option preserving the metric is obtained via spherical harmonics and the corresponding linear mapping is given by the formulae [15]:

$$\begin{aligned}
 D_{xx} &= \frac{3}{35}(9D_{xxxx} + 8D_{xxyy} + 8D_{xxzz} - D_{yyyy} - D_{zzzz} - 2D_{yyzz}) \\
 D_{yy} &= \frac{3}{35}(9D_{yyyy} + 8D_{xxyy} + 8D_{yyzz} - D_{xxxx} - D_{zzzz} - 2D_{xxzz}) \\
 D_{zz} &= \frac{3}{35}(9D_{zzzz} + 8D_{xxzz} + 8D_{yyzz} - D_{xxxx} - D_{yyyy} - 2D_{xxyy}) \\
 D_{xy} &= \frac{6}{7}(D_{xxyy} + D_{yyyx} + D_{zzxy}) \\
 D_{xz} &= \frac{6}{7}(D_{xxxz} + D_{zzzx} + D_{yyxz}) \\
 D_{yz} &= \frac{6}{7}(D_{yyyz} + D_{zzzy} + D_{xxyz})
 \end{aligned} \tag{9}$$

The formulation of this reduction given by equation (9) is consistent as mean diffusivity is proportional as follows:

$$\text{trace}(T^{(2)}) = \frac{3}{5} \text{trace}(T^{(4)}) \tag{10}$$

The reader is referred to [15] for details.

C. Flattening of 4th order tensor

Another approach to describe 4th order tensors is by unfolding the tensor, arranging the tensor as a matrix. Thus, a general r th order tensor $T^{(r)}$ can be expressed as a matrix of $(r-2)$ nd order tensors:

$$T^{(r)} = \begin{pmatrix} T_{xx}^{(r-2)} & T_{xy}^{(r-2)} & T_{xz}^{(r-2)} \\ T_{yx}^{(r-2)} & T_{yy}^{(r-2)} & T_{yz}^{(r-2)} \\ T_{zx}^{(r-2)} & T_{zy}^{(r-2)} & T_{zz}^{(r-2)} \end{pmatrix} \tag{11}$$

We deal with $r = 4$, but our discussion is extendable to higher orders. The diagonal components of this representation are SPD [34]. Thus, we obtain 3 2nd order SPD out of one 4th order tensor. Choosing the coordinates to diagonalize one of them leaves 15 free parameters, exactly as for the 4th order tensors. This method is called the diagonal component (DC) projection.

IV. RIEMANNIAN MANIFOLD CLUSTERING

For processing the fields of 3D and 6D 2nd order tensors, we use the so called affine and Log-Euclidean (LogE) metrics [24]. Exponential map is a function that maps each symmetric matrix to an SPD. The inverse of the exponential map is the logarithmic map. We may use these inverse mapping at each fixed SPD matrix p . Several authors discussed various metrics suitable for statistics explored in imaging, see [24] for a survey, including the spectral similarity measures. The affine invariant metric is the natural metric of the Riemannian symmetric space, but it is computationally slow with involvements of inverse, square root and logarithmic operations. Moreover, this metric has limitation like swelling effect. The geodesic distance between two SPD tensors p, x is computed as

$$d_A(p, x) = \|\text{Log}_p(x)\|. \tag{12}$$

In the ambient Euclidean space, the SPD matrices lie in the interior of a convex cone and the affine metric turns it into a complete Riemannian manifold. See [37] for more information.

The LogE metric is due to [35]. This metric is based upon the observation that matrix exponential of symmetric

matrices is diffeomorphic to the space of SPDs. For two SPD matrices p_1, p_2 ,

$$d_{\text{LogE}}(p_1, p_2) = \|\log(p_1) - \log(p_2)\|. \tag{13}$$

The studies [24][35][36] also indicate that LogE metric is better in preserving anisotropy measure. The white matter is modelled as a tensor with an anisotropy. This measure is crucial in evaluation of statistics of tensors, white matter tractography and segmentation. The spectral similarity measures perform even better, but we are using the affine and LogE metrics to compare the projections here.

We use the Lapacian Eigen Map (LE) for projecting the non linear data to lower dimension. For this projection affinity matrix is computed as:

$$w_{ij} = \exp\left(-\frac{\text{dist}(p_i, p_j)^2}{\sigma^2} - \frac{\|i - j\|^2}{w_e}\right) \tag{14}$$

The first term evaluates affinity between data in Riemannian space whereas the 2nd term provides similarity in the image space (with $\|i - j\|$ being a suitably blown-up Euclidean distance ensuring robustness with respect to noise). These terms ensure extraction of the fiber structure from the background. The variance is evaluated respecting the log-normal distribution of the SPD diffusion tensor data [34]. The coefficient w_e is experimentally chosen and depends upon the size of window.

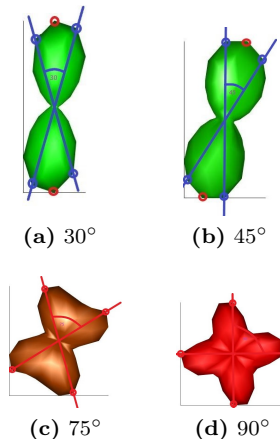


Fig. 1: 4th order ODF with various angle differences between the two fibers

V. EXPERIMENT AND RESULTS

We simulated synthetic images (64 Gradient direction with $b=1500 \text{ s/mm}^2$) using adaptive kernel method [38]. The Fig. 1 (a)-(d) shows 4th order tensor ODF where angle difference between the two fibers are $30^\circ, 45^\circ, 75^\circ$ and 90° . The maxima of these ODFs does not necessarily align with actual underlying fibers. Another issue with these ODFs is fuzziness in the maxima. If we observe Fig.1 (a) and (b) the pointing circle in red indicates the maxima at angles in between the range. These maxima are at wrong position, right positions are indicated by the blue circle. Fig. 3 displays fiber orientation error in the presence of Rician noise at various angle differences between the two fibers. The vertical bar shows standard deviation for 50

TABLE I: Execution time for DC vs. CT-FOD methods

Comparison Table														
Angle between underlying fibers	Difference	00	10	20	30	40	50	60	70	80	90	100	110	120
Time in Sec	DC Method	0.0014	0.0013	0.0011	0.0012	0.0095	0.0001	0.0001	0.0001	0.0002	0.0001	0.0001	0.0001	0.0001
	CT ODFs	3.1437	1.7980	2.0849	1.6177	1.6555	2.0732	2.0209	2.0216	2.1774	1.6799	2.0444	2.1078	2.1189

TABLE II: Segmentation of the fiber and background (Dice coefficient)

Metric	Method/ Rician Noise Level	Back Ground					Fiber 1				
		0.00	0.02	0.04	0.06	0.08	0.00	0.02	0.04	0.06	0.08
Affine	3D Mapping	1.000	0.994	0.995	0.998	0.998	1.000	0.970	0.973	0.995	0.995
	6D Mapping	0.937	0.984	0.950	0.985	0.953	0.874	0.937	0.862	0.940	0.860
LogE	3D Mapping	0.967	0.983	0.975	0.996	0.984	0.906	0.939	0.909	0.955	0.911
	6D Mapping	0.948	0.982	0.967	0.956	0.949	0.852	0.937	0.844	0.911	0.875

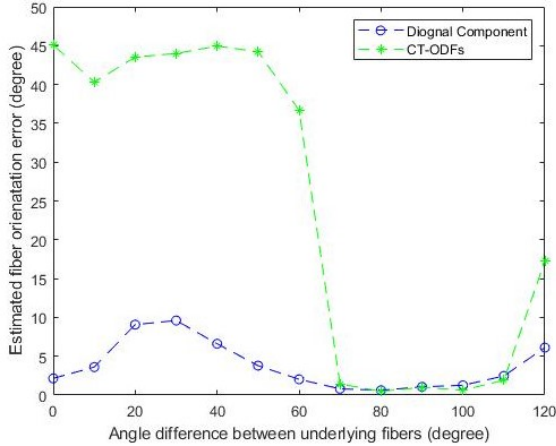


Fig. 2: Comparison of DC vs. CT-FOD

repeated experiments at each level of noise. The principal eigenvectors of the diagonal components (DC) can discern directions of maximum diffusion.

The CT-FOD method is based on the signal deconvolution [17]. This approach uses a subroutine to find maxima of the reoriented ODFs. We compared evolution of such maxima with our method. These maxima are directions of prominent diffusion directions. We generated ODFs for two fibers crossing at known angles and estimated fiber orientation error due to the DC and CT-FOD approach. The

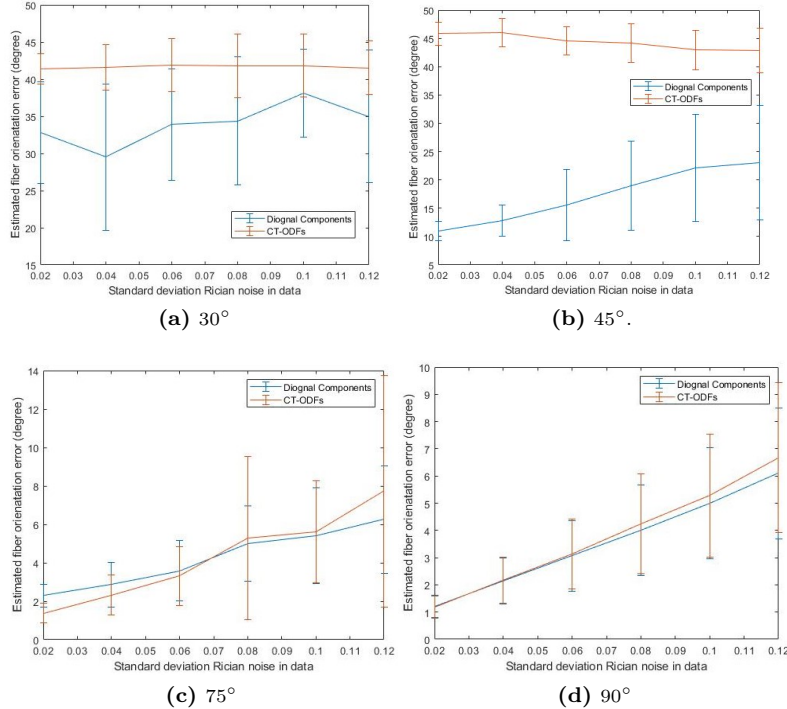
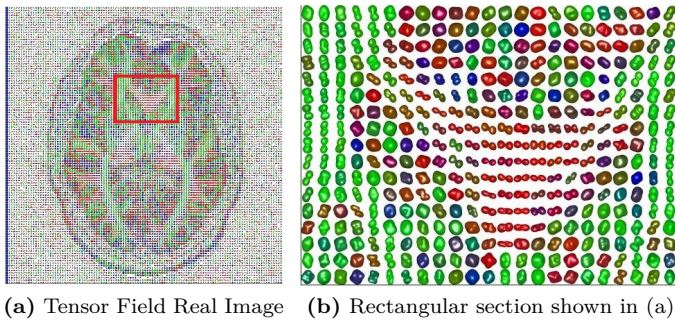
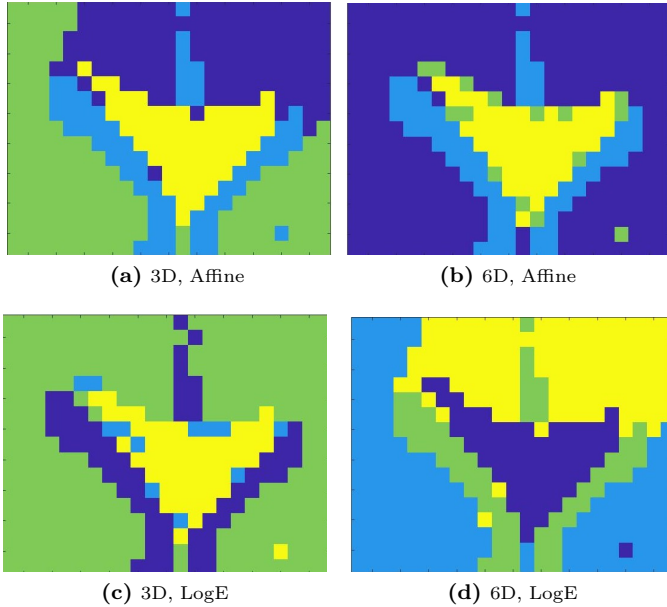


Fig. 3: Standard deviation of orientation error in the presence of Rician noise



(a) Tensor Field Real Image (b) Rectangular section shown in (a)

Fig. 4: Real Image



(a) 3D, Affine

(b) 6D, Affine

(c) 3D, LogE

(d) 6D, LogE

Fig. 5: Segmentation result

comparison is shown in Fig. 2. The performance of both the methods is similar within angle-difference range 70° - 110° but for angle-differences outside this range the DC method performs better than CT-FOD. In all cases, the DC method shows lower orientation errors. As we approach within the above range their performances converge.

Table I displays the relative execution time. This experiment is conducted on machine with 16 GB RAM and Processor Intel(R) Core(TM) i5-7500 CPU @ 2.70GHz 2.71GHz. The DC method is about 10^3 times faster. The independent 15 coefficients are arranged at fixed positions, thus computation of the three diagonal components is straightforward. Consequently, it jumps the optimization step which needs to find the maxima of ODF in CT-FOD method.

Table II shows average segmentation results in terms of Dice coefficients under various levels of Rician noise. We created a data bank of 30 synthetic configurations having one (curved/linear) fiber. The performance of 3D 2nd order mapping with affine metric is slightly better than all other combinations. We performed similar tests including crossing fibers with different complexities. The comparison of the projections and metrics results in the same conclusion.

We have also performed similar tests on real images. See

Fig. 4, 5 for one example. Again, the 3D 2nd order affine metric choice outperforms the others.

VI. CONCLUSION

The experiments have shown that the 6D projection of 4th order tensors is more sensitive to noise than the 3D projection. Previous work of the authors [34] showed that the 3D DC projections, together with the spectral metrics perform, even better.

In segmentation application, crossing regions are considered as a unit, therefore, the orientation of individual fibers has no effect on the outcome. The diagonal components of the flattened 4th order tensor effectively reveal the directions of maximum diffusion. We are looking forward to see how the eigenvectors of these components can be used in tracking the fibers in heterogeneous regions.

DISCLOSURES

No conflicts of interest, financial or otherwise, are declared by the authors.

ACKNOWLEDGMENT

The first three authors have been supported by the grant MUNI/A/0885/2019 of Masaryk University, Jan Slovak gratefully acknowledges support from the Grant Agency of the Czech Republic, grant Nr. GA17-01171S. The authors would like to thank Lubomir Vojtisek for providing real diffusion-weighted MRI data and acknowledge the core facility MAFIL of CEITEC supported by the MEYS CR (LM2018129 Czech-Bioimaging).

REFERENCES

- [1] P. C. Lauterbur *et al.*, "Image formation by induced local interactions: examples employing nuclear magnetic resonance," 1973.
- [2] P. J. Basser, J. Mattiello, and D. LeBihan, "Estimation of the effective self-diffusion tensor from the nmr spin echo," *Journal of Magnetic Resonance, Series B*, vol. 103, no. 3, pp. 247–254, 1994.
- [3] P. J. J. Mattiello, and D. LeBihan, "Mr diffusion tensor spectroscopy and imaging," *Biophysical journal*, vol. 66, no. 1, pp. 259–267, 1994.
- [4] V. J. Wedeen, P. Hagmann, W.-Y. I. Tseng, T. G. Reese, and R. M. Weisskoff, "Mapping complex tissue architecture with diffusion spectrum magnetic resonance imaging," *Magnetic resonance in medicine*, vol. 54, no. 6, pp. 1377–1386, 2005.
- [5] A. Leemans, B. Jeurissen, J. Sijbers, and D. Jones, "Exploredti: a graphical toolbox for processing, analyzing, and visualizing diffusion mr data," in *Proc Intl Soc Mag Reson Med*, vol. 17, 2009, p. 3537.
- [6] P. T. Fletcher, "Geodesic regression and the theory of least squares on riemannian manifolds," *International journal of computer vision*, vol. 105, no. 2, pp. 171–185, 2013.
- [7] P. T. Fletcher and S. Joshi, "Principal geodesic analysis on symmetric spaces: Statistics of diffusion tensors," in *Computer Vision and Mathematical Methods in Medical and Biomedical Image Analysis*. Springer, 2004, pp. 87–98.
- [8] P. T. Fletcher, C. Lu, and S. Joshi, "Statistics of shape via principal geodesic analysis on lie groups," in *2003 IEEE Computer Society Conference on Computer Vision and Pattern Recognition, 2003. Proceedings.*, vol. 1. IEEE, 2003, pp. I–I.
- [9] K. Krajsek, M. I. Menzel, and H. Scharr, "A riemannian bayesian framework for estimating diffusion tensor images," *International Journal of Computer Vision*, vol. 120, no. 3, pp. 272–299, 2016.
- [10] X. Pennec, P. Fillard, and N. Ayache, "A riemannian framework for tensor computing," *International journal of computer vision*, vol. 66, no. 1, pp. 41–66, 2006.

- [11] C. Lenglet, M. Rousson, R. Deriche, O. Faugeras, S. Lehericy, and K. Ugurbil, "A riemannian approach to diffusion tensor images segmentation," in *Biennial International Conference on Information Processing in Medical Imaging*. Springer, 2005, pp. 591–602.
- [12] A. Barmpoutis, M. S. Hwang, D. Howland, J. R. Forder, and B. C. Vemuri, "Regularized positive-definite fourth order tensor field estimation from dw-mri," *NeuroImage*, vol. 45, no. 1, pp. S153–S162, 2009.
- [13] A. Barmpoutis and B. C. Vemuri, "A unified framework for estimating diffusion tensors of any order with symmetric positive-definite constraints," in *2010 IEEE international symposium on biomedical imaging: from nano to macro*. IEEE, 2010, pp. 1385–1388.
- [14] E. Özarslan and T. H. Mareci, "Generalized diffusion tensor imaging and analytical relationships between diffusion tensor imaging and high angular resolution diffusion imaging," *Magnetic Resonance in Medicine: An Official Journal of the International Society for Magnetic Resonance in Medicine*, vol. 50, no. 5, pp. 955–965, 2003.
- [15] M. Moakher, "Fourth-order cartesian tensors: old and new facts, notions and applications," *The Quarterly Journal of Mechanics & Applied Mathematics*, vol. 61, no. 2, pp. 181–203, 2008.
- [16] C. Liu, R. Bammer, and M. E. Moseley, "Limitations of apparent diffusion coefficient-based models in characterizing non-gaussian diffusion," *Magnetic Resonance in Medicine: An Official Journal of the International Society for Magnetic Resonance in Medicine*, vol. 54, no. 2, pp. 419–428, 2005.
- [17] Y. T. Weldeselassie, A. Barmpoutis, and M. S. Atkins, "Symmetric positive semi-definite cartesian tensor fiber orientation distributions (ct-fod)," *Medical Image Analysis*, vol. 16, no. 6, pp. 1121–1129, 2012.
- [18] H. E. Çetingül, M. J. Wright, P. M. Thompson, and R. Vidal, "Segmentation of high angular resolution diffusion mri using sparse riemannian manifold clustering," *IEEE transactions on medical imaging*, vol. 33, no. 2, pp. 301–317, 2013.
- [19] H. E. Cetingül and R. Vidal, "Sparse riemannian manifold clustering for hardi segmentation," in *2011 IEEE International Symposium on Biomedical Imaging: From Nano to Macro*. IEEE, 2011, pp. 1750–1753.
- [20] L. Jonasson, X. Bresson, J. Thiran, V. J. Wedeen, and P. Hagmann, "Representing diffusion mri in 5-d simplifies regularization and segmentation of white matter tracts," *IEEE Transactions on Medical Imaging*, vol. 26, no. 11, pp. 1547–1554, 2007.
- [21] L. T. Skovgaard, "A riemannian geometry of the multivariate normal model," *Scandinavian Journal of Statistics*, pp. 211–223, 1984.
- [22] D. Tschumperle and R. Deriche, "Diffusion tensor regularization with constraints preservation," in *Proceedings of the 2001 IEEE Computer Society Conference on Computer Vision and Pattern Recognition. CVPR 2001*, vol. 1. IEEE, 2001, pp. I–I.
- [23] D. S. Tuch *et al.*, "Diffusion mri of complex tissue structure," Ph.D. dissertation, Massachusetts Institute of Technology, 2002.
- [24] S. KAUSHIK, "Geometric approach to segmentation in diffusion magnetic resonance imaging [online]," Dissertation, Masaryk University, Faculty of Science, Brno, 2020 [cited 2020-08-03]. [Online]. Available: [AvailablefromWWW<https://is.muni.cz/th/thsvd/>](https://is.muni.cz/th/thsvd/)
- [25] P. J. Basser and S. Pajevic, "A normal distribution for tensor-valued random variables: applications to diffusion tensor mri," *IEEE Transactions on Medical Imaging*, vol. 22, no. 7, pp. 785–794, 2003.
- [26] S. Pajevic and P. J. Basser, "Parametric and non-parametric statistical analysis of dt-mri data," *Journal of magnetic resonance*, vol. 161, no. 1, pp. 1–14, 2003.
- [27] G. K. Batchelor and I. Proudman, "The large-scale structure of homogenous turbulence," *Philosophical Transactions of the Royal Society of London. Series A, Mathematical and Physical Sciences*, vol. 248, no. 949, pp. 369–405, 1956.
- [28] H. Wu and J. M. Lees, "Cartesian parametrization of anisotropic traveltime tomography," *Geophysical Journal International*, vol. 137, no. 1, pp. 64–80, 1999.
- [29] L. Walpole, "Fourth-rank tensors of the thirty-two crystal classes: multiplication tables," *Proceedings of the Royal Society of London. A. Mathematical and Physical Sciences*, vol. 391, no. 1800, pp. 149–179, 1984.
- [30] A. Bóna, I. Bucataru, and M. A. Slawinski, "Characterization of elasticity-tensor symmetries using $su(2)$," *Journal of Elasticity*, vol. 75, no. 3, pp. 267–289, 2004.
- [31] S. C. Cowin, "Properties of the anisotropic elasticity tensor," *The Quarterly Journal of Mechanics and Applied Mathematics*, vol. 42, no. 2, pp. 249–266, 1989.
- [32] M. M. Mehrabadi and S. C. Cowin, "Eigentensors of linear anisotropic elastic materials," *The Quarterly Journal of Mechanics and Applied Mathematics*, vol. 43, no. 1, pp. 15–41, 1990.
- [33] A. Tarantola, *Elements for physics: quantities, qualities, and intrinsic theories*. Springer Science & Business Media, 2005.
- [34] S. Kaushik and J. Slovák, "Hardi segmentation via fourth-order tensors and anisotropy preserving similarity measures," *Journal of Mathematical Imaging and Vision*, vol. 61, pp. 1221 – 1234, 2019.
- [35] V. Arsigny, P. Fillard, X. Pennec, and N. Ayache, "Log-euclidean metrics for fast and simple calculus on diffusion tensors," *Magnetic Resonance in Medicine: An Official Journal of the International Society for Magnetic Resonance in Medicine*, vol. 56, no. 2, pp. 411–421, 2006.
- [36] A. Collard, S. Bonnabel, C. Phillips, and R. Sepulchre, "An anisotropy preserving metric for dti processing," *arXiv preprint arXiv:1210.2826*, 2012.
- [37] P. T. Fletcher and S. Joshi, "Riemannian geometry for the statistical analysis of diffusion tensor data," *Signal Processing*, vol. 87, no. 2, pp. 250–262, 2007.
- [38] B. J. Barmpoutis and B. C. Vemuri, "Adaptive kernels for multi-fiber reconstruction," *Information processing in medical imaging : proceedings of the conference*, vol. 21, pp. 338–49, 2009.
- [39] M. Descoteaux, E. Angelino, S. Fitzgibbons, and R. Deriche, "Apparent diffusion coefficients from high angular resolution diffusion imaging: Estimation and applications," *Magnetic Resonance in Medicine: An Official Journal of the International Society for Magnetic Resonance in Medicine*, vol. 56, no. 2, pp. 395–410, 2006.